Steel and Composite Structures, *Vol. 22, No. 2 (2016) 323-352*
DOI: http://dx.doi.org/10.12989/scs.2016.22.2.323

Strength and stiffness modeling of extended endplate connections with circular and rectangular bolt configurations

Elie G. Hantouche [*] and Elie N. Mouannes [a]

Department of Civil and Environmental Engineering, Faculty of Engineering and Architecture, American University of Beirut (AUB), Beirut, Lebanon

(*Received October 19, 2015, Revised June 16, 2016, Accepted October 11, 2016*)

Abstract. The results of a series of finite element (FE) simulations and experimental studies are used to develop strength and stiffness models that predict the failure capacity and response characteristics of unstiffened extended endplate connections with circular and rectangular bolt configurations associated with deep girders. The proposed stiffness models are composed of multi-linear springs which model the overall extended endplate/column flange system deformation and strength of key-components. Comparison of model predictions with FE and experimental results available in the literature show that the proposed models accurately predict the strength and the response of extended endplate/column system with circular and rectangular bolt configurations. The effect of the bolt configuration (circular and rectangular) on the prying phenomenon encountered in the unstiffened extended endplate/column system was investigated. Based on FE results, extended endplate with circular bolt configuration has a more ductile behavior and exhibits higher total prying forces. The proposed models can be used to design connections that cover all possible failure modes for extended endplate with circular bolt configuration. This study provides guidelines for engineers to account for the additional forces induced in the tension bolts and for the maximum rotational capacity demand in the connection which are required for seismic analysis and design.

Keywords: extended endplate; failure modes; circular bolts; finite element; strength and stiffness models; ductility

1. Introduction

Extended endplate connections have become the choice of many structural engineers in designing connections for moment resisting frames in seismic areas. Extensive experimental and analytical work on full-scale extended endplate connections was performed during the past three decades. Previous research work and experimental tests were developed to provide guidelines and recommendations for the design of extended endplate connections. Studies on the behavior of extended endplate connections for improving the ductility and strength of the connection were conducted earlier by Sumner and Murray (2002), Kiamanesh *et al*. (2013), and recently conducted by Akgőnen *et al*. (2015) and Ghassemieh *et al*. (2015).

Previous studies considered that the endplate thickness is a major parameter that affects the

∗Corresponding author, Ph.D., Assistant Professor, E-mail: eh12@aub.edu.lb
[a] Master's Student, E-mail: enm03@mail.aub.edu

http://www.techno-press.org/?journal=scs&subpage=6 ISSN: 1229-9367 (Print), 1598-6233 (Online)

stiffness of the connection and its global response (Kukreti *et al*. 1987, Katula and Dunai 2015, Liu and Wang 2015). Also, continuity plates are often used in extended endplate/column systems to stiffen the column flange and web, in order to resist large forces transmitted by the beam flange. On the other hand, detailing columns without continuity plates reduces the cost and effort needed for fabrication. The deformation contributing from the column flange which causes an additional bolt force in the absence of continuity plates was not explicitly addressed in the design of extended endplate connection. Also, previous work was limited to extended endplate connections having rectangular bolts configuration. Until recently, studies performed by Kiamanesh *et al*. (2013), Schweizer (2013), and Morrison *et al*. (2015) showed that positioning the bolts in a circular pattern around the flange alters the distribution of the tensile force, and therefore increases the overall capacity and ductility of the connection. Note that no design guidelines and recommendations were proposed for extended endplate having circular bolt configuration.

One of the main behavioral characteristics of extended endplate connections in predicting the ultimate strength and response is the prying phenomenon. Total prying is defined as the amount of tensile force that is added to the bolts due to a significant deformation of extended endplate/ column flange system. In particular, secondary prying is defined as the additional force induced in the tension bolts due to excessive column flange deformation (Hantouche *et al*. 2012). Several component models for predicting the ultimate strength and response are reported in the literature and the important ones include those suggested by Faella *et al*. (1997), Swanson (2002), Piluso *et al*. (2001), Rassati *et al*. (2004), Pucinotti (2001), Hu *et al*. (2012), Coelho *et al*. (2004), Eurocode 3 (2005), Piluso and Rizzano (2008), Lemonis and Gantes (2009) and recently Hantouche *et al*. (2015) and Bai *et al*. (2015). No existing models available in the literature are able to predict the prying effect on the response of eight bolted unstiffened extended endplate connection having circular bolt patterns. Therefore, it is necessary to quantify the amount of prying forces due to bending of endplate (*primary prying*) and column flange deformation (*secondary prying*).

In this paper, proposed strength and stiffness models based on multi-linear spring approach are developed to predict strength and deformation of isolated components with circular and rectangular bolt configurations. The proposed models are validated against experimental results available in the literature. With its simplicity in application when compared to other numerical methods (i.e., FE analysis), the proposed models are used to design extended endplate connections with circular and rectangular bolt configurations. It is noted that the model accounts for the extended endplate/column flange system deformation and does not include the beam and column web deformation (full-scale level). Based on FE results, the prying phenomenon and bolts response in extended endplate connections with circular and rectangular bolt patterns are examined. The behavioral characteristics of a typical extended endplate/column system with circular bolts configuration for use in seismic design are investigated.

2. Preliminary design of extended endplate connection with rectangular and circular bolt configurations

Eight bolted extended endplate connections with circular and rectangular bolt configurations are designed and detailed using guidelines available in the AISC 358-10 (AISC 2010). The extended endplate is welded to the beam and the beam/endplate system is field bolted to the column flange (see Fig. 1(a)). A rectangular matrix of 8 bolts (2 columns and 4 rows) is provided at the level of each beam flange as shown in Fig. 1(b). The connection is designed such that the

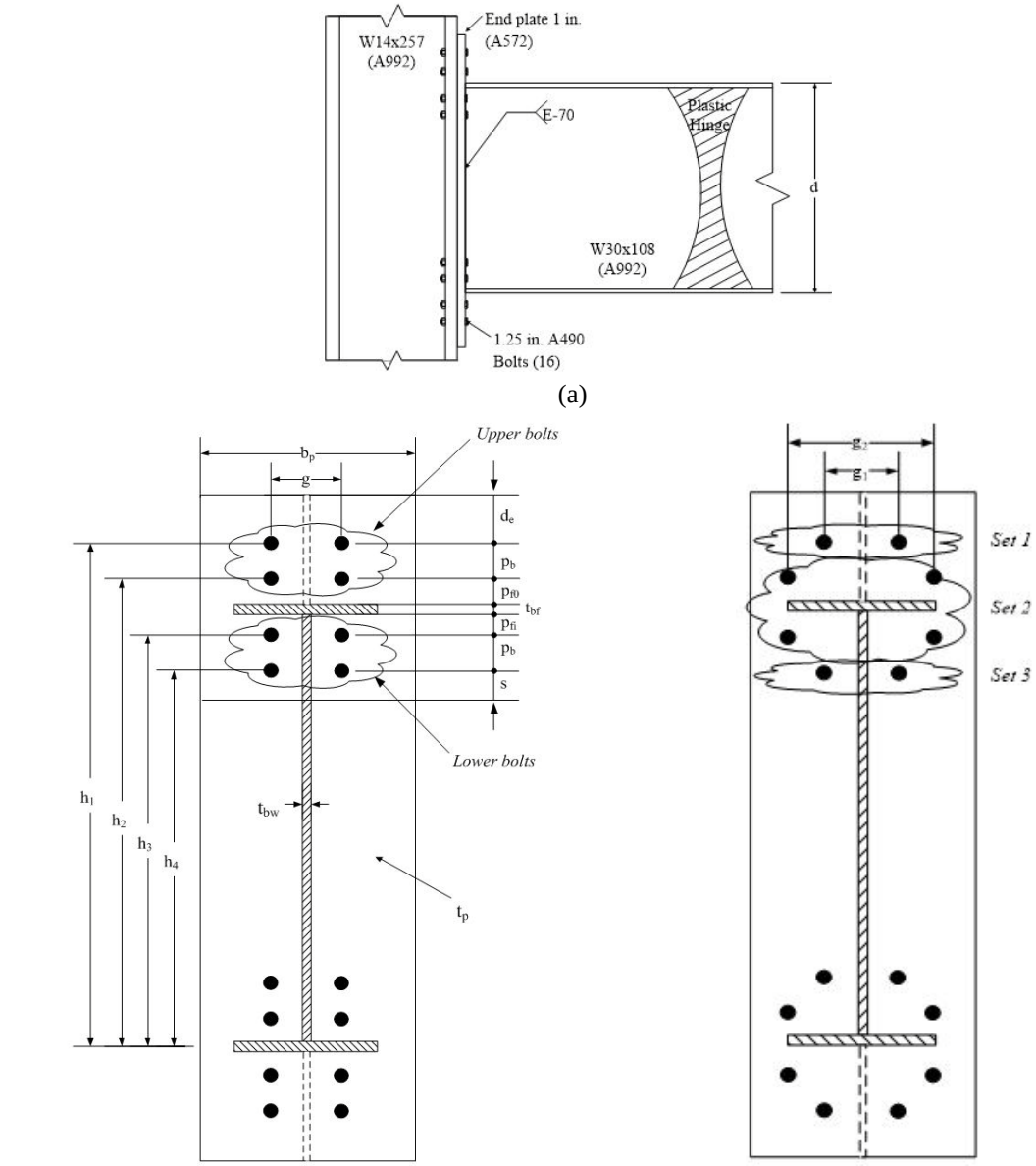

(b) Extended endplate with rectangular bolt configuration (c) Extended endplate with circular bolt configuration

Fig. 1 Extended endplate connection with circular and rectangular bolts configuration

plastic hinge occurs in the beam at a distance, *d*, from the face of the column. Note that the beam and column are made of A992 steel, the plate material is made of A572 with A490 bolts. The beam is designed as a seismically compact element.

The connections considered in the design consist of W24×76 and W30×108 beams connected to columns with the flange thicknesses, t_{cf}, varying from 1.9 cm (0.75 in.) to 4.8 cm (1.89 in.). The preliminary connection configuration is based on the following steps:

(1) First identify the independent geometric parameters of the extended endplate. Select values for the gauge distances (g, p_{fi}, p_{fo}, p_b, d_e, b_p) shown in Fig. 1(b) within the range of acceptable values given in Table 6.1 of the AISC 358-10 (AISC 2010). Note that the geometric parameters are defined in Chapter 6 in the AISC 358-10 (AISC 2010). After choosing the geometric parameters, h_i (mm) can be calculated (see Fig. 1(b)).
(2) Assume there is no prying. Determine the minimum bolt diameter d_b (cm), with capacity to resist the applied moment at the face of the support M_f.
(3) Select the extended endplate thickness, t_p (mm), based on endplate yielding mechanism. Select the minimum required thickness to the nearest 0.3 cm (1/8 in.).
(4) The endplate should not extend from the top of the beam flange by more than 12.7 cm (5 in.), avoiding any local buckling behavior at both edges of the plate.

For the circular bolt configuration, the designer would start with a preliminary rectangular bolt design, and then proceed in accordance to the proposed assumptions and modifications:

(1) It is assumed to have equal gage distance ($p_{fo} = p_{fi}$) for the bolts to get a perfectly symmetrical circular configuration.
(2) The bolt gage distances shown in Fig. 1(c) are calculated as $g_1 = (b_p - 2e) / 2$ and $g_2 = b_p - 2e$, where b_p (cm) is the plate width and e (cm) is the minimum edge distance defined in section J of the AISC 360-10 (AISC 2010).
(3) The 4 far bolts (*Sets 1 and 3*) are moved vertically, rearranged on the circle centered at the beam flange and passing by the bolts in *Set 2* giving a symmetric circular configuration as shown in Fig. 1(c).
(4) The minimum bolt spacing requirements are in accordance to section J in the AISC 360-10 (AISC 2010).

3. Geometric parameters of extended endplate connection and cases selected for analysis

The independent geometric and force related parameters for extended endplate connections are identified. The endplate thickness t_p, the column flange thickness t_{cf}, and the bolts vertical gages h_i reflected by the bolts arrangement are three geometric parameters that impact the amount of prying and deformation in extended endplate connections. The force-related parameter is the applied tension load T on the extended endplate resulting from the moment applied at the beam tip. The minimum required thickness of the extended endplate, t_p, was calculated based on the applied moment encountered in the beam. Furthermore, two types of columns were investigated, ranging from rigid columns (column flange is thicker than the endplate), to flexible columns (column flange thinner than the endplate). The study covers columns with flange thicknesses, t_{cf}, ranging from 1.9 cm (0.75 in.) to 4.7 cm (1.89 in.). Every case is associated with an extended endplate having circular and rectangular bolt patterns to study the effect of bolt distribution on the response. Note that, the endplate thickness, t_p, is a dependent parameter, incorporated in the design according to the existing design restrictions defined in the AISC 358-10 (AISC 2010).

Therefore, in order to study the amount of total prying in endplate/column systems for a given load T, a total of twenty eight extended endplates (14 with rectangular bolts pattern and 14 with circular bolts pattern) are studied and listed in Table 1.

Table 1 Test matrix

Column flange thickness, (t_{cf})	Endplate thickness (t_p)	Tension bolt diameter (d_b)
Design details for W24×76 beam		
1.90 cm ($\frac{3}{4}$ in.)	2.54 cm (1.00 in.)	2.85 cm ($1\frac{1}{8}$ in.)
2.15 cm (0.85 in.)	2.54 cm (1.00 in.)	2.85 cm ($1\frac{1}{8}$ in.)
2.54 cm (1.00 in.)	2.54 cm (1.00 in.)	2.85 cm ($1\frac{1}{8}$ in.)
3.17 cm ($1\frac{1}{4}$ in.)	2.54 cm (1.00 in.)	2.85 cm ($1\frac{1}{8}$ in.)
3.80 cm ($1\frac{1}{2}$ in.)	2.54 cm (1.00 in.)	2.85 cm ($1\frac{1}{8}$ in.)
4.44 cm ($1\frac{3}{4}$ in.)	2.54 cm (1.00 in.)	2.85 cm ($1\frac{1}{8}$ in.)
4.80 cm (1.89 in.)	2.54 cm (1.00 in.)	2.85 cm ($1\frac{1}{8}$ in.)
Design details for W30×108 beam		
1.90 cm ($\frac{3}{4}$ in.)	2.54 cm (1.00 in.)	3.17 cm ($1\frac{1}{4}$ in.)
2.15 cm (0.85 in.)	2.54 cm (1.00 in.)	3.17 cm ($1\frac{1}{4}$ in.)
2.54 cm (1.00 in.)	2.54 cm (1.00 in.)	3.17 cm ($1\frac{1}{4}$ in.)
3.17 cm ($1\frac{1}{4}$ in.)	2.54 cm (1.00 in.)	3.17 cm ($1\frac{1}{4}$ in.)
3.80 cm ($1\frac{1}{2}$ in.)	2.54 cm (1.00 in.)	3.17 cm ($1\frac{1}{4}$ in.)
4.44 cm ($1\frac{3}{4}$ in.)	2.54 cm (1.00 in.)	3.17 cm ($1\frac{1}{4}$ in.)
4.80 cm (1.89 in.)	2.54 cm (1.00 in.)	3.17 cm ($1\frac{1}{4}$ in.)

4. Three dimensional solid extended endplate model

Using ABAQUS, three-dimensional (3-D) FE models were developed for typical extended endplate connection test specimen which incorporate the following characteristics: (1) nonlinear material behavior for base and bolt material; (2) full pretensioning of fasteners; and (3) contact interaction between the extended endplate and column flange, bolt head and column flange, and bolt nut and endplate.

The FE modeling technique described in this section is to be used (1) for validation against experimental results available in Sumner and Murray (2002), and Schweizer (2013); and (2) for running FE simulations to develop strength and stiffness models that predict the response and strength of extended endplate connection having rectangular and circular bolts arrangement.

4.1 Mesh design

Eight-node linear brick shape elements with reduced integration (C3D8R) were used to mesh the endplate/column system. Fig. 2 shows a full 3-D model representing the extended endplate/column system with rectangular bolts configuration. At the connection region, where failure is likely to occur, a smaller mesh size is used (see Fig. 2). Moreover, to account for stress concentrations around the bolt-holes, a mapped meshing technique was used to discretize bolts and their surrounding areas. The length of the column was equal to 305 cm (120 in.).

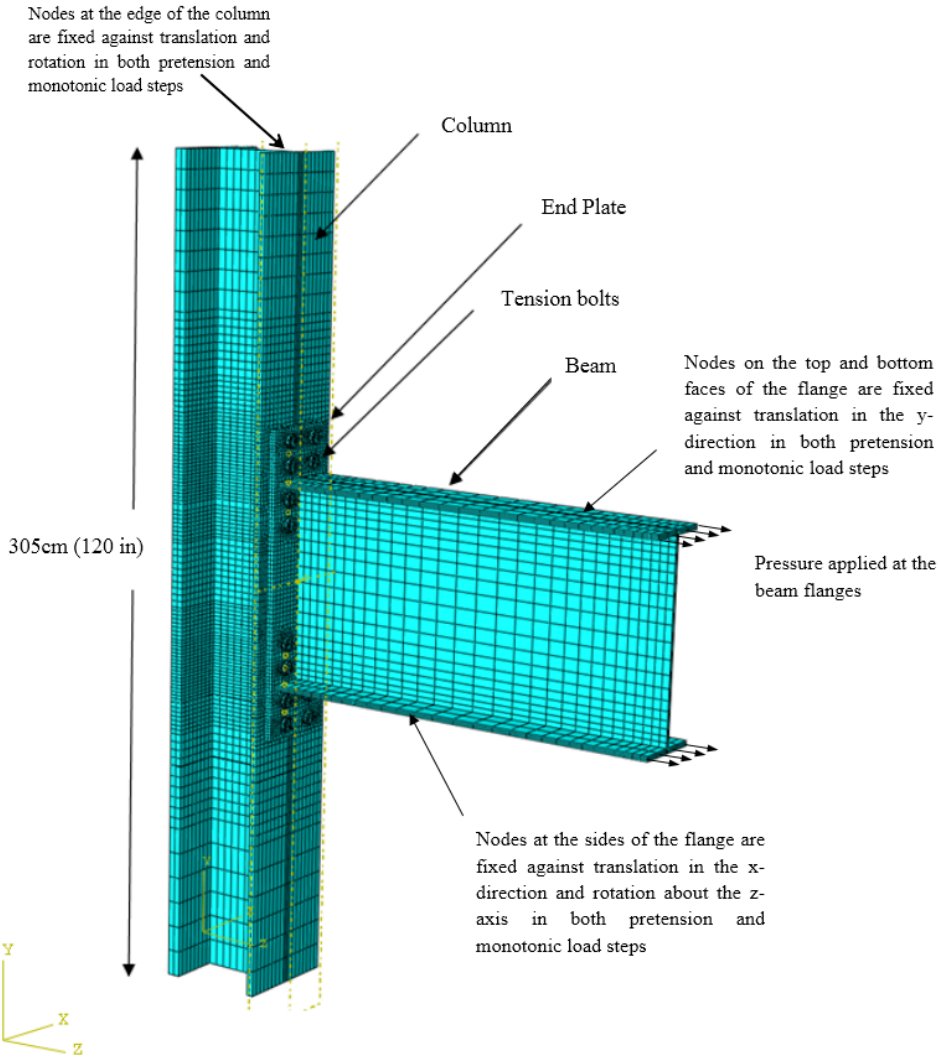

Fig. 2 Three-dimensional model of endplate connection with rectangular bolt configuration

The model consists of a column, a beam, an endplate and 16 tension bolts. The beam is attached to the endplate using tie constraint representing the CJP welds in order to allow full load transfer between the elements. The tie constraint fuses together two elements having different mesh constitution. The interaction between the plate, bolt head, bolt shank and column flange are modeled as surface to surface contact with finite sliding and a coefficient of friction equal to 0.2, consistent with previous models developed in Hantouche *et al*.(2012).

4.2 Material properties

The von Mises yield criterion is used in the analysis. The bolts were modeled on ABAQUS using their gross area, rather than their effective area. A490 bolts are modeled with a yield stress of 811 MPa (117.5 kips) and an ultimate stress of 872 MPa (126.5 kips). The yield strain, was

0.00405 and the ultimate plastic strain, was 0.03084. The yield and ultimate stress used for the base material are 385 MPa (55 ksi) and 500 MPa (71.5 ksi), respectively. The yield strain used for the base material is 0.00189, and its plastic strain is 0.09827. For all the steel members of the connection, Young's modulus was assumed as E = 203,000 MPa (29000 ksi), and Poisson's ratio as υ = 0.30. A bilinear stress strain model with isotropic hardening for both base and bolt material was used in the analysis.

4.3 Boundary conditions and loading

The analysis was divided into two steps: (1) pretension step, where the 16 bolts are pretensioned to the minimum required force defined in the AISC 360-10 (AISC 2010); and (2) loading step, where the monotonic load is applied at the beam tip. In the pretension and loading steps, the degrees of freedom of the column edge are constrained against any translation and rotation. The lateral sides of the beam flange are assumed to be fixed against translation along the x-direction. The outer and inner faces of the beam flange are fixed against translation in the y-direction to avoid any bending action on the connection (see Fig. 2). To compute the net primary prying force, Q_p, the column flange is assumed to be fully rigid and is fully constrained against any translation and rotation. However, the column flange is free to deform when computing the total prying force, Q_T.

During the first step, the pretensioning force is generated by applying a bolt body force at the shank cross section equal to the minimum pretension force. Throughout the loading step, surface pressure is applied on the flange section at the beam tip (see Fig. 2).

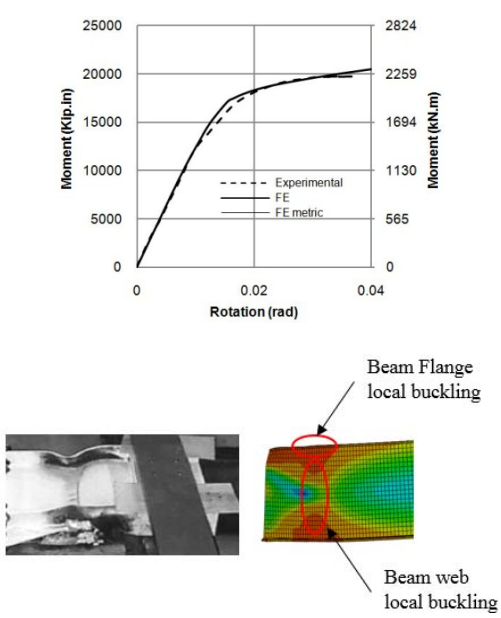

(a) Extended endplate with rectangular bolt configuration moment-rotation curves: FE vs. Experimental (Sumner and Murray 2002)

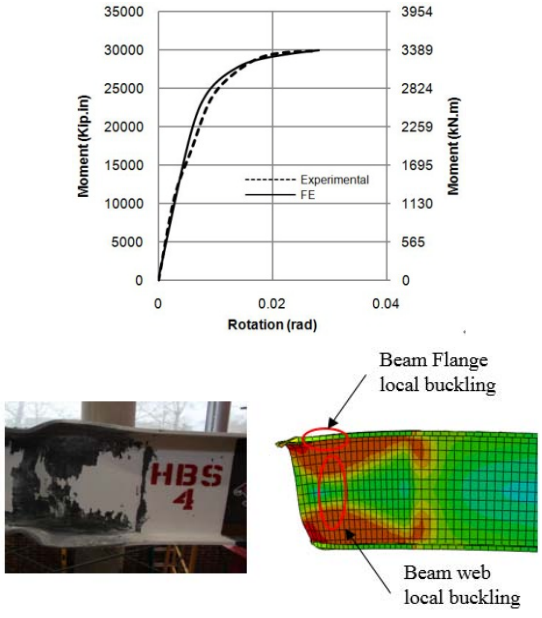

(b) Extended endplate with circular bolt configuration moment-rotation curves: FE vs. Experimental. (Schweizer 2013)

Fig. 3 Finite element versus experimental results

5. Validation with experimental results

Two FE models of extended endplate connections with rectangular and circular bolt configurations were developed to reproduce experimental results available in the literature. Figs. 3(a) and (b) show a comparison of the FE moment-rotation curve and failure modes with experimental results of Sumner and Murray (2002), and Schweizer (2013), respectively. Furthermore, Figs. 4(a) and (b) show the FE and experimental results of the bolt force versus moment curves of the near and far bolts respectively, of the extended endplate connection with circular bolts configuration. The FE model accurately predicts the experimental moment-rotation envelope curve as far as stiffness, strength and ductility. In addition, the FE models exhibited similar failure modes as described in the experimental results. The FE model developed in this study to reproduce the experimental results performed by Sumner and Murray (2002) shows that beam flange and web local buckling occurs in the endplate connection with rectangular bolt pattern. The ductile failure mode is associated with yielding of the beam as shown in the FE results (see Fig. 3(a)). The FE model developed in this study to reproduce the experimental results conducted by Schweizer (2013) shows that buckling of the beam flange and web occurs in the extended endplate connection with circular bolt configuration as shown in Fig. 3(b). It can be seen that the endplate is still in its elastic range; however yielding occurs in the bolts which conforms to the experimental results reported in Schweizer (2013). Hence, it can be concluded that the FE modeling technique can be used to develop extended endplate models with rectangular and circular bolt configurations for the parametric study.

6. Investigation of primary and secondary prying

This study investigates the prying phenomenon in extended endplate/column systems with circular and rectangular bolt configurations that should be addressed in designing full-strength connections. More importantly, this study highlights the effect of the circular bolt arrangement on prying forces in extended endplate connections.

6.1 Data analysis

The prying force is calculated at the step where the first bolt row fails causing the failure of the connection. Note that yielding of the bolt shank is assumed to be the failure criteria of the first component. The bolt force exhibited in every bolt B is calculated by multiplying the von Mises stresses by the gross section area of the bolt shank. The prying force, Q, is calculated by subtracting the total bolt force B from the total applied force, T, at failure: $Q = B\text{-}T$. Two models were generated on ABAQUS to calculate the secondary prying, Q_S. In the first model, the column flange is free to deform used to calculate the total prying, Q_T. The second model was developed to calculate the primary prying Q_P with rigid column flange. The percentage secondary prying (Q_S / T) is obtained by subtracting the primary prying (Q_p / T) from the total prying (Q_P / T) at the same load step T where failure occurs, as shown in Eq. (1).

$$\left(\frac{Q_s}{T}\right)=\left(\frac{Q_T}{T}\right)-\left(\frac{Q_p}{T}\right) \tag{1}$$

7. Results

7.1 Prying phenomenon

FE models of extended endplate connection with various column flange thicknesses having circular and rectangular bolt configurations were analyzed under monotonic loading. The primary and secondary prying forces and the associated percentage of prying with respect to the total applied load was calculated for each column flange thickness for the W24×76 and W30×108 beams as shown in Table 2.

The extended endplate/column system with circular bolt configuration exhibited higher total prying forces for all the studied cases. The total prying exhibited from the system is the added contribution of primary prying (generated from the plate deformation) and secondary prying forces (induced by the excessive column flange deformation). For the cases associated with very thin column flanges ($t_{cf} \leq 2.1$ cm), the percentage of total prying exceeded 100% as shown in Table 2. This is due to the significant deformation of the column flange which caused additional forces in the tension bolts.

Endplate connections with circular bolt pattern associated with W24×76 and W30×108 beams exhibited lower secondary prying forces (Table 2). On the other hand, endplate with rectangular bolt configuration exhibited lower primary prying forces when compared to its circular counterpart. More generally, as the column flange thickness increases, the secondary prying force decreases in both endplates with circular and rectangular bolt configurations.

Table 2 Percentage of primary and secondary prying and prying force for W24×76 and W30×108 beams

		W24×76				W30×108			
		Circular		Rectangular		Circular		Rectangular	
t_{cf} (cm)	Prying	Percent prying (%)	Prying force (Kips)	Percent prying (%)	Prying force (Kips)	Percent prying (%)	Prying force (Kips)	Percent prying (%)	Prying force (Kips)
1.9	Primary	85	663	60	529	100	814	66	703
	Secondary	34	265	39	344	43	350	54	575
2.1	Primary	72	590	50	477	90	930	66	733
	Secondary	28	230	30	286	32	330	47	522
2.5	Primary	60	510	43	462	69	855	55	690
	Secondary	25	212	26	279	25	310	39	488
3.2	Primary	58	493	48	456	71	941	56	758
	Secondary	7	59	9	85	13	172	18	243
3.8	Primary	59	550	57	547	65	873	53	718
	Secondary	0	0	0	0	10	134	14	189
4.4	Primary	58	640	57	547	65	845	52	712
	Secondary	0	0	0	0	7	130	11	150
4.8	Primary	57	650	57	550	66	905	57	764
	Secondary	0	0	0	0	0	0	0	0

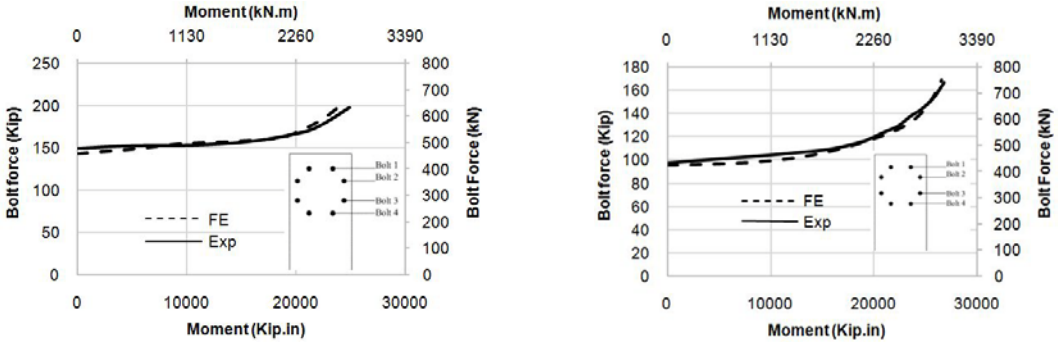

(a) Extended endplate with circular bolt configuration far bolt force (Bolt 1) versus moment curves: FE vs. Experimental (Schweizer 2013)

(b) Extended endplate with circular bolt configuration near bolt force (Bolt 2) versus moment curves: FE vs. Experimenta (Schweizer (2013))

Fig. 4 Finite element versus experimental results of bolt force versus beam end moment

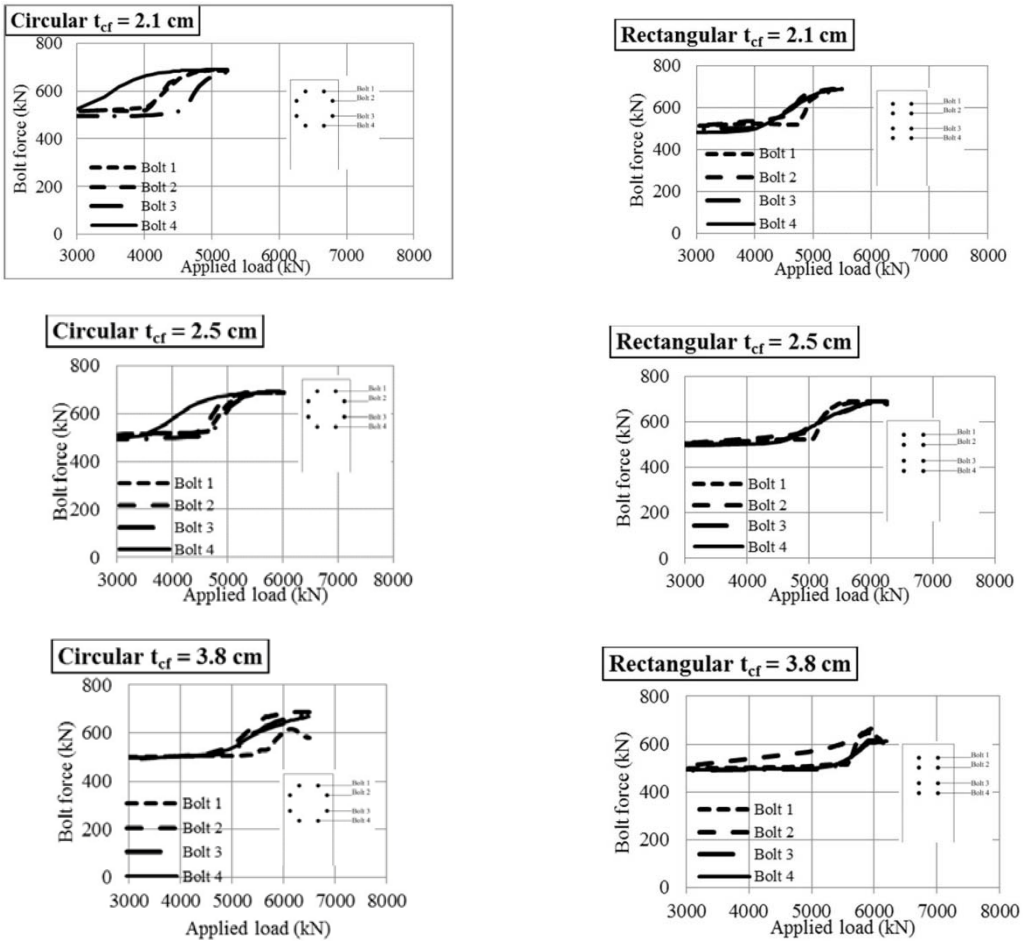

Fig. 5 Bolt force history for extended endplate with rectangular and circular bolt configurations

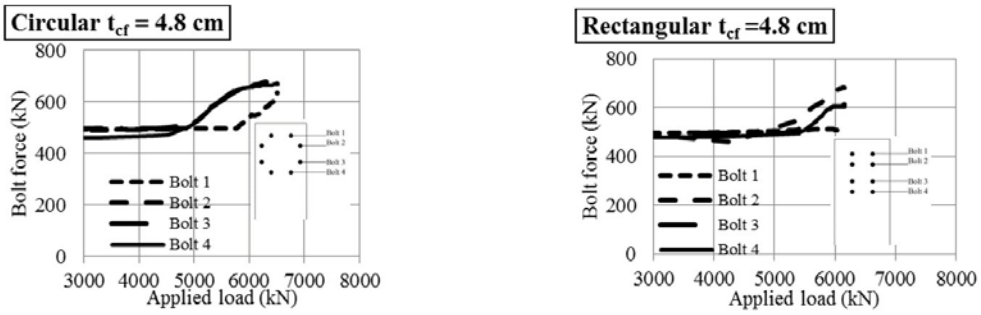

Fig. 5 Continued

7.2 Bolt force variation

To further investigate the effectiveness of the circular bolt pattern, the bolt force history was investigated for extended endplate connections having circular and rectangular bolt configurations with t_{cf} equal to 2.1, 2.5, 3.8 and 4.8 cm as shown in Fig. 5. It can be seen that for all column/endplate system with circular bolt configurations, the far bolts (*Bolts 4*) are involved in carrying the load earlier and more effectively than *Bolts 4* in rectangular bolt configurations. In connections with circular bolt pattern, the far bolts (*Bolt 4*) carry more load than the near bolts (*Bolts 2 and 3*), which are subject to higher bending moments in rectangular bolt configuration and carry more load than the other bolts (*Bolts 1*, *4*). In rectangular bolt configuration, *Bolts 3* and *4* follow the same loading history, since their curves overlap. The two bolts are stiffened by the beam web; they are subject to equal deformations and stress distribution. In contrast, in connections with circular bolt configuration the force is equally spread across the bolts. Furthermore, in connections with rectangular bolt configurations where t_{cf} = 4.8 cm, the unstiffened far bolt (*Bolt 1*) carries no additional force above pretension load, when the beam is loaded, while in its counterpart connection with circular bolt configuration, all bolts are engaged. Hence in circular connection, the load is efficiently spread across the bolts, developing a more ductile behavior. The bolt force of the sixteen tension bolts was calculated as a percentage of their ultimate tensile strength. In the circular bolt pattern, the bolts are more effective and reach higher capacity than the bolts in the connection with rectangular bolt configurations. Finally, in connections with rectangular and circular patterns *Bolt 1* exhibited similar bolt force history in thin columns. However, the near bolts (*Bolts 2* and *3*) become more effective and reach their ultimate capacity with thicker columns (t_{cf} = 4.8 cm).

8. Strength models

The FE and experimental results are used to develop strength models to predict the capacity of extended endplate and column flange with circular and rectangular bolt configurations. Four possible failure modes are addressed: (1) formation of a plastic hinge at the K-zone (see Fig. 6) followed by fracture of the interior tension bolts; (2) formation of a plastic hinge at the first bolt line followed by fracture of the interior tension bolt; (3) full plastification at the K-zone; and (4) pure tension bolt fracture.

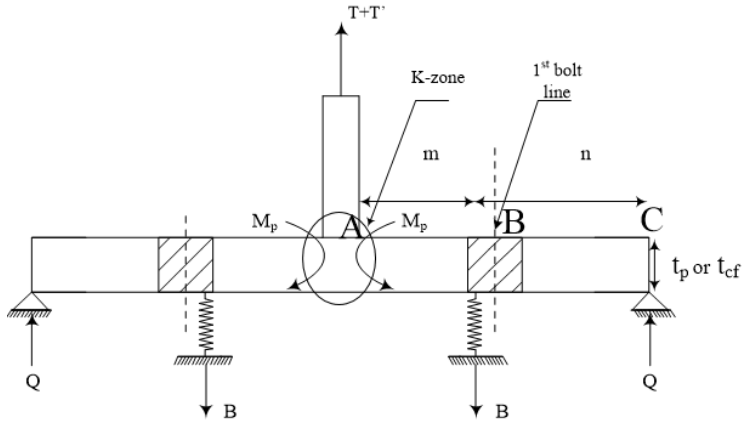

(a) End plate with circular bolt or column flange with circular and rectangular bolt configurations geometry

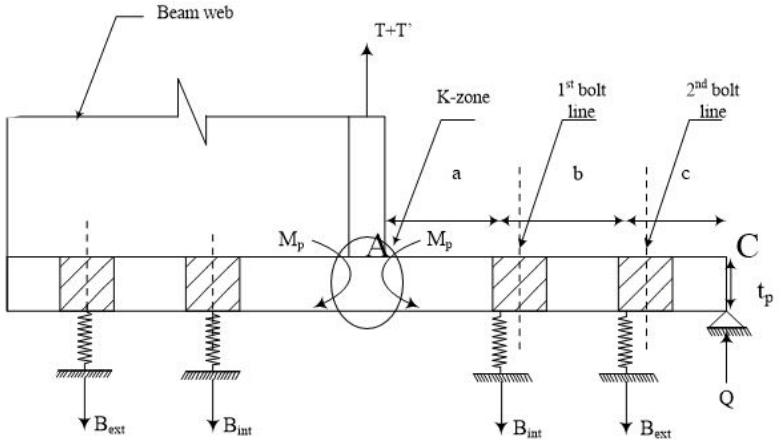

(b) Endplate with rectangular bolt configuration geometry

Fig. 6 End plate column flange with circular and rectangular bolt configurations geometry

8.1 Strength models for circular bolts arrangement

8.1.1 Extended endplate with circular bolt configuration

Strength models for extended endplate connections with circular bolt configuration were not addressed in previous studies. The FE results show that extended endplate connection with circular bolt configuration exhibit high primary prying force, hence it is deemed necessary to quantify the endplate's capacity. The endplate was modeled as strip beam element for the plate, and springs to model the bolts. The von Mises stress contours obtained from the FE analysis of the selected cases show that no full plastification of the extended endplate at the K-zone is developed. Thus, the problem is considered statically indeterminate and an additional relationship that relates the prying force to the applied load is needed to solve the problem. A partial yielding model for extended endplate connections with circular bolt configuration is needed to predict the endplate capacity. A detailed parametric study was performed to limit the range of endplate partial yielding. Geometric parameters that impact the plate yielding are found to be the radius of the concentric bolt pattern, *r*,

and the thickness of the plate, t_p. From the FE results, partial yielding developed in extended endplate with t_p, ranging from 3 cm (1.2 in.) to 4.3 cm (1.7 in.). A dimensionless ratio which involves the radius of the concentric bolts to the plate thickness r/t_p has a major impact on the amount of yielding encountered in the plate. Seven endplate FE models were analyzed and a linear relationship is fitted to the FE results, as shown in Fig. 7 to obtain an analytical model for prediction of the primary prying force when partial yielding occurs followed by yielding of the bolts. The best fit linear equation obtained for $2.80 \leq r/t_p \leq 5.00$ covering practical ranges

$$\frac{Q_p}{T} = 24\left(\frac{r}{t_p}\right) - 54 \tag{2}$$

Considering the bolt force equal to γB_n, and by substituting $B=Q+T$ in Eq. (2) the capacity per bolt can be written as follows

$$T = \frac{\gamma B_n}{0.24\left(\frac{r}{t_p}\right) + 0.46} \tag{3}$$

where γ is assumed to be equal to 0.8 to account for bending of the tension bolts and B_n (kN) is the nominal bolt tensile strength. Note that the bolts are not only subject to tension forces but are also subject to bending. The proposed strength model is validated against previous work performed by Kiamanesh *et al*. (2013) and predicts a capacity of 3,552 kN (800 kips) for W30×99 beam with r/t_p = 4.87. This is around 4.7% difference when comparing with the FE results. Hence the proposed model predicts with excellent agreement the capacity of the extended endplate with circular bolt configuration.

8.1.2 Column flange with circular bolt configuration

The 8 tension bolts were divided into three *Sets* according to their behavior as shown in Fig. 1(c). The proposed strength model consists of a spring representing the bolts and a beam element for the column flange as shown in Fig. 6(a).

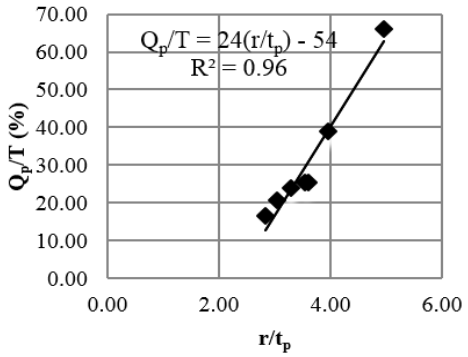

Fig. 7 Primary prying relationship

The FE models cover the range of column flange thicknesses varying from 1.9 cm (0.75 in.) to 4.8 cm (1.89 in.). For thin column flanges where t_{cf} is less than 2.54 cm (1 in.), flange mechanism occurs in *Sets 1* and *3*, and mixed mode failure occurs in *Set 2*. However for thick column flanges, where t_{cf} is greater than 2.54 cm (1 in.), mixed mode failure occurs in *Sets 1*, *2* and *3*.

Mixed mode failure capacity is calculated as follows

$$T = T' = \frac{\gamma B_n n}{m+n} + \frac{M_p}{m+n} \tag{4}$$

Flange mechanism capacity is calculated as follows

$$T = T' = \frac{(1+\delta)M_p}{m} \tag{5}$$

where

$$\delta = 1 - \frac{d_h}{p} \tag{6}$$

$$M_p = \frac{p t_{cf}^2}{4} F_y \tag{7}$$

where, T (kN) is the applied force, M_p (kN.m) is the plastic moment, d_h (cm) is the bolt hole diameter, p (cm) is the tributary width of a pair of tension bolts, F_y (MPa) is the yield stress, m (cm) is the length of the column flange measured from the inside edge of the bolt to the location of occurrence of the plastic hinge at the K-zone, n (cm) is the length measured from the inside edge of the bolt line to the outside edge of the column flange, where contact with the endplate occurs as shown in Fig. 6(a), and δ is the ratio of the net area at the center of the bolt line to the area of the beam flange. The bolt force is assumed to be applied at a distance d_b / 2 from the bolt hole centerline. The tributary width per bolt, p, used in computing the plastic moment, M_p, is reflected by the effective length of the column, W_c. The effective length is limited by the regions on the column flange, where von Mises stress is not significant (see Fig. 8). The effective length varies with the column flange thickness; the thicker the column flange the smaller the deformation. Therefore, there is no average length that can be considered when computing W_c. A linear relationship relating W_c and t_{cf} is derived based on 8 FE models of extended endplates having rectangular or circular bolt patterns

$$W_c = -40 t_{cf} + 195 \geq 142 \; cm \tag{8}$$

A linear relationship is obtained from the best fit of the FE results for the studied cases. The tributary width, p, can be calculated as follows

$$p = \frac{17 W_c - 835}{n_b} \text{ (cm/bolt)} \tag{9}$$

The proposed strength model predicts a capacity of 5,843 kN for W30×99 beam associated

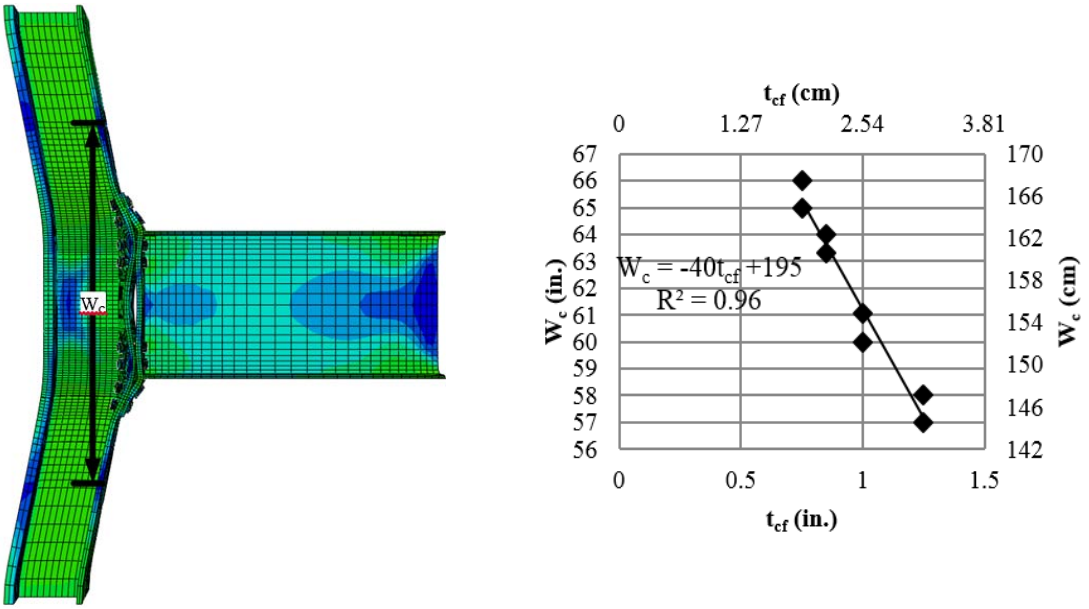

(a) FE model (b) Column effective length vs. Column flange thickness

Fig. 8 Column effective length (W_c)

with W14×194 thick column having a t_{cf} equal to 3.65 cm (1.43 in.) studied in Kiamanesh *et al*. (2013). This is around 1% less than the reported results. The proposed strength model predicts with excellent agreement the capacity of the column flange with circular bolt configuration.

8.2 Strength models for rectangular bolt configuration

8.2.1 Extended endplate with rectangular bolt configuration

A strength model is developed to predict the primary prying capacity exhibited in the extended endplate with rectangular bolt configuration. Two vertical strips were modeled at the level of each flange as shown in Fig. 6(b), accounting for the beam web stiffening effect. At failure of the connection, mixed mode occurs at the *upper bolts* lines (see Fig. 1(b)). However, at the *lower bolts* level, (see Fig. 1(b)), the beam web acts as a stiffener, hence the bending of the plate is negligible, and the plate separates completely from the column flange as shown in Fig. 9. Therefore, the force developed at the *lower bolts*, T', is equal to

$$T' = \gamma n_b \xi B_n / 8 \tag{10}$$

where the reduction factor ($\xi = 0.75$) is used to account for the beam web stiffening effect and n_b is the number of the tension bolts. The strength associated with the *upper bolts* is derived from previous models available in the literature. For mixed mode failure at the *upper bolts* level (plastic hinge develops at the K-zone followed by interior bolt fracture)

$$T = \frac{\gamma B_n c}{a+b+c} + \frac{\gamma B_n (b+c)}{a+b+c} + \frac{M_p}{a+b+c} \tag{11}$$

$$M_p = \frac{pt_p^2}{4} F_y \tag{12}$$

$$p = \frac{8b_p}{n_b} \tag{13}$$

where, T (kN) is the applied forces, a (cm) is the length of the plate measured from the inside edge of the interior bolt to the location of occurrence of the plastic hinge at the K-zone, b (cm) is the gage distance between the tension bolts, and c (cm) is the length measured from the inside edge of the exterior bolt line to the outside edge of the endplate as shown in Fig. 6(b). The proposed strength model results, revealed a capacity of 5,931 kN and 5,514 kN for extended endplate with rectangular bolt configuration associated with W30×108 and W24×76 beams, respectively. This is around 1% and 8% more than the strength predicted by the FE results. For validation purposes, the proposed model is validated against FE simulations reported in Kiamanesh *et al*. (2013). The proposed model predicts a capacity of 3,383 kN. The percentage difference is around 3.5% when compared with results available in Kiamanesh *et al*. (2013), for the extended endplate (t_p = 2.54 cm) associated with W30×99 beam.

8.2.2 Column flange with rectangular bolt configuration

The column flange is subdivided into 4 horizontal strips consisting of 2 bolts each as modeled in Fig. 6(a). From the FE results, the governing failure modes are: (1) full plastification of the flange followed by bolt fracture; and (2) tension bolt fracture. Full flange plastification occurs when t_{cf} varies between 1.9 cm (0.75 in.) to 3.2 cm (1.25 in.) and tension bolt fracture occurs when t_{cf} varies between 3.2 cm (1.25 in.) to 4.8 cm (1.89 in.), where complete plate separation occurs. The capacity for tension bolts fracture, when full separation occurs, can be calculated as $T = T' = \gamma\xi B_n$, and when full plastification occurs (plastic hinge develops at the K-zone followed by plastification of interior and exterior bolt lines)

$$T = T' = \frac{(1+\delta)M_p}{m} \tag{14}$$

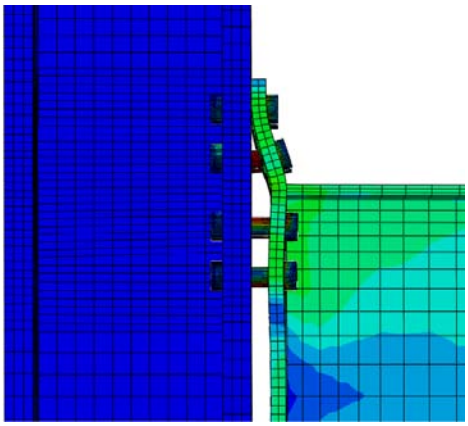

Fig. 9 Deformation of the extended endplate with rectangular bolt configuration

where p is calculated as per Eq. (9), m (cm) is the length of the column flange measured form the inside of the bolt to the location of the plastic hinge at the K-zone as shown in Fig. 6(a).

The proposed strength model predicts a capacity of 5,260 kN for a W30×108 beam connected to a W14×194 column which is 7% more when comparing with the FE results. In addition the model predicts a capacity of 5,336 kN (1,202 kips) for a W14×257 column connected to a W24×76 beam, which is 4% more when comparing with the FE results. Hence, the proposed strength model predicts with reasonable agreement the capacity of the column flange associated with deep beams when compared with the FE results.

9. Column flange strength prediction using yield-line analysis

A yield-line analysis is developed to predict the yield strength of the column flange having circular bolt configuration. A governing yield-line mechanism is identified for column flange with circular bolt configuration. The virtual work method is used to compute the minimum required column flange thickness, t_{cf}, of a given yield-line pattern, based on the principle of conservation of energy.

Based on yield-line theory, the governing yield-line pattern for column flange having circular bolt configuration is presented in Fig. 10. The internal work W_i can be computed as follows

$$W_i = 2M_p\left[4\left(\frac{b_{cf}}{2s}\right)+4\left(l+2p_b\right)\frac{1}{g_2}+8\left(p_b+s\right)\frac{1}{g_1}\right] \tag{15}$$

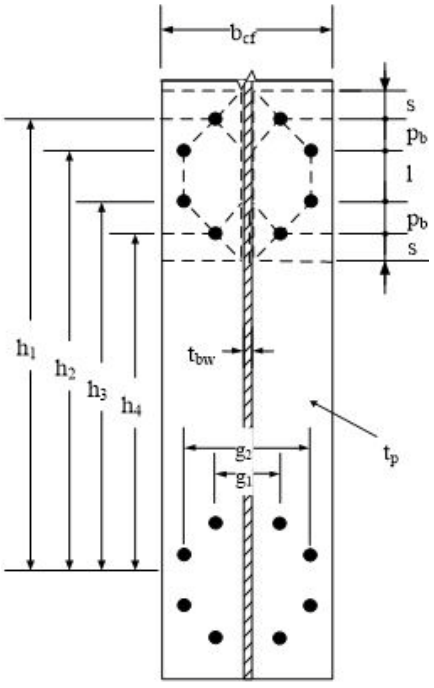

Fig. 10 Yield line mechanism for column flange with circular bolt configuration

Where b_{cf}, s, l, p_b, g_2, g_1, are geometric parameters defined in Fig. 10. The external work done by the system is equal to $W_e = F_u \cdot 1$ where F_u is equal to the ultimate load at failure. The connection strength based on yielding of the column flange is found by equating the external energy with the internal energy. The minimum required column flange thickness, t_{cf} is computed as follows

$$t_{cf} \geq \sqrt{\frac{F_u}{\left[2\left(\frac{b_{cf}}{2s}\right)+2\left(l+2p_b\right)\frac{1}{g_2}+4\left(p_b+s\right)\frac{1}{g_1}\right]F_{yc}}} \tag{16}$$

where F_{yc} (MPa) is the yield stress of the column. According to Eq. (16), the required minimum column flange thickness for extended endplate associated with W30×108 beam connected to a W14×257 column is computed as $t_{cf} \geq 3.48$ cm (1.37 in.). The distance s, can be calculated by differentiating the internal work with respect to s and equating to zero

$$s = \frac{1}{2}\sqrt{b_{cf} g_1} \tag{17}$$

According to the AISC 358-10 (AISC 2010), the required minimum column flange thickness for the same connection is computed as $t_{cf} \geq 2.90$ cm (1.14 in.).

10. Stiffness modeling

The experimental and FE results of extended endplate connections with circular and rectangular bolt configurations are used to develop a stiffness model. The model is based on multi-linear springs which model deformations of key component elements from tension bolt elongation, bending of the plate, column flange deformation including primary and secondary prying forces. Modeling the endplate is complex because all of these mechanisms interact with one another and hence simple strength checks cannot provide the necessary stiffness, ductility information required for seismic design.

10.1 Bolt stiffness model

The bolt stiffness model proposed by Hantouche *et al*. (2013) is used to model the tension bolts throughout the loading history of the extended endplate. The bolt stiffness model is composed of four linear segments. The first segment models the bolt in the pretension step, the second segment models the bolt in the elastic range, the third segment models the bolt after first yielding has been reached and the fourth segment models the bolt in the plastic range. The elastic bolt stiffness K_b (kN/cm) is calculated as follows (Swanson 2002)

$$\frac{1}{K_b} = \frac{fd_b}{A_b E} + \frac{L_s}{A_b E} + \frac{fd_b}{A_{be} E} \tag{18}$$

where, f is the stiffness correlation factor, A_b (cm^2) is the nominal area of the bolt shank, A_{be} (cm^2) is the effective area of the threads and L_s (cm) is the free shank length of the bolt.

10.2 Extended endplate/column system with circular bolt configuration

10.2.1 Extended endplate with circular bolt configuration

The proposed stiffness model consists of the extended endplate associated with deep beams having an endplate thickness, t_p, less than 3.00 cm (1.2 in.). From the FE results, full plastification develops at the *upper bolt* line (see Fig. 1(b)), followed by endplate separation at the *lower bolts* level at failure of the bolts. A decision tree showing different endplate limit states (*Upper bolts* strip) is shown in Fig. 11(a). At the *upper bolts* level shown in Fig. 1(b), the stiffness model was developed in accordance to the far bolts geometry (see Fig. 6(a)). The subscript used in the stiffness coefficients reflects the state of the endplate and *upper bolt*. For instance, $K_{ee,k}$ is the

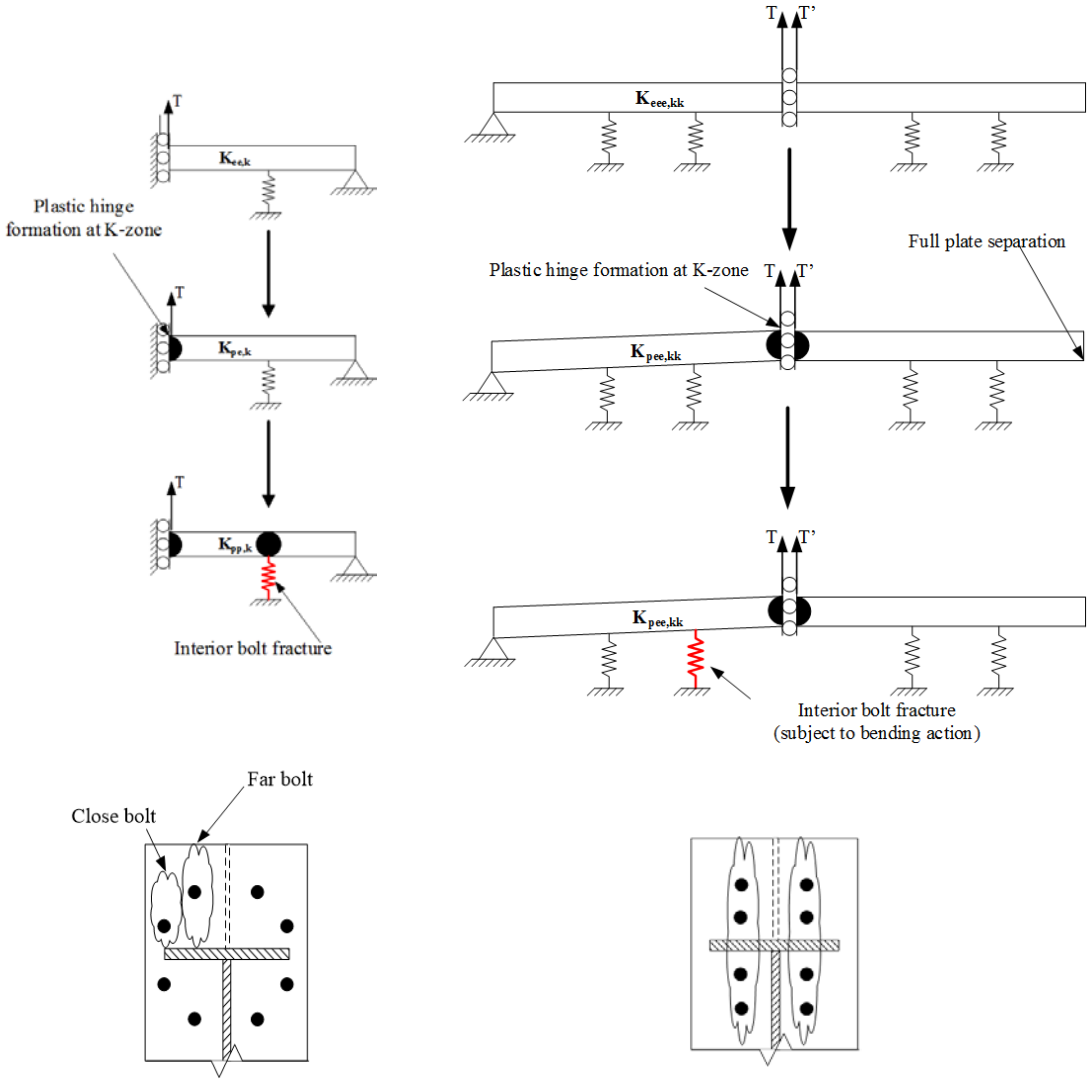

(a) Circular bolt configuration (b) Rectangular bolt configuration

Fig. 11 Decision tree for extended endplate connection

stiffness of the endplate that is totally elastic, with the bolt in its kth state. $K_{pe,k}$ is the stiffness of the endplate when the plastic hinge has formed at the K-zone and the bolt line is still in its elastic range, $K_{pp,k}$ is the final stiffness of the endplate when the bolt line and the K-zone are in their plastic state and full plastification occurs in the endplate. The stiffness was derived using direct stiffness method and is presented in the following equations accounting for shear deformation. Strain hardening which occurs after plastic hinge formation was modeled by a rotational spring with constants K_{h1} and K_{h2} according to Douty and McGuire (1965). The hinge depth was set equal to the thickness of the endplate. The mechanistic equations are developed below

$$K_{ee,k} = \frac{12EI(3EI + K_{b,k}\Omega_3)}{\gamma_{ee,k}} \tag{19}$$

$$Q_{ee,k} = \frac{18EI(K_{b,k}mn^2\beta_b - 2EI)}{\gamma_{ee,k}} \tag{20}$$

$$\gamma_{ee,k} = 12EI\Omega_1 + K_{b,k}\Omega_2 \tag{21}$$

$$K_{pe,k} = \frac{12EI(3EI(K_{b,k}n^2 + K_{h1}) + K_{b,k}K_{h1}\Omega_3)}{\gamma_{pe,k}} \tag{22}$$

$$Q_{pe,k} = \frac{18EI(2EI(K_{b,k}mn - K_{h1}) + K_{b,k}K_{h1}nm^2\beta_b)}{\gamma_{pe,k}} \tag{23}$$

$$\gamma_{pe,k} = 12EI(K_{h1}\Omega_1 + K_{b,k}(m^3n^2\beta_a + m^2n^3\beta_b) + 3EI\Omega_4) + K_{b,k}K_{h1}\Omega_2 \tag{24}$$

$$K_{pp,k} = \frac{K_{h1}K_{h2} + K_{b,k}n^2(K_{h1} + K_{h2})}{\gamma_{pp,k}} \tag{25}$$

$$Q_{pp,k} = \frac{K_{h2}(K_{b,k}mn - K_{h1})}{\gamma_{pp,k}} \tag{26}$$

$$\gamma_{pp,k} = K_{h2}\Omega_4 + K_{h1}n + K_{b,k}m^2n^2 \tag{27}$$

where

$$\Omega_1 = \beta_b(m^3 + 3nm^2 + 3n^2m) + n^3\beta_a \tag{28}$$

$$\Omega_2 = 3n^2m^4{\beta_b}^2 + 4n^3m^3\beta_a\beta_b \tag{29}$$

$$\Omega_3 = n^3\beta_a + 3n^2m\beta_b \tag{30}$$

$$\Omega_4 = n^2 + 2mn + m^2 \tag{31}$$

$$p = \frac{b_p}{4} \tag{32}$$

$$I = \frac{pt_p^3}{12} \tag{33}$$

$$\beta_a = 1 + \frac{12EI}{Gpt_p n^2} \tag{34}$$

$$\beta_b = 1 + \frac{12EI}{Gpt_p m^2} \tag{35}$$

$$K_{h1} = \frac{EI}{t_p} \tag{36}$$

$$K_{h2} = \left(1 - \frac{d_h}{p}\right)\frac{EI}{t_p} \tag{37}$$

where I (cm^4) is the moment of inertia, G (kN/cm^2) is the shear modulus of elasticity, $K_{b,k}$ (kN/cm) is the bolt stiffness at the k^{th} step, β_a, β_b, Ω_1, Ω_2, Ω_3 and Ω_4 are constants used in the calculation of the extended endplate stiffness and $\gamma_{ee,k}$, $\gamma_{ep,k}$ are constants used in the calculation of $K_{ee,k}$, m (cm) is the length of the endplate measured from the inside edge of the bolt line to the K-zone and n (cm) is the length of the endplate measured from the inside edge of the bolt line to the outside edge of the endplate as shown in Fig. 6(a). The stiffness K and prying gradient, Q, were derived to be used in an incremental solution technique. An engineer would start by determining the stiffness, $K_{ij,k}$ and the prying gradient $Q_{ij,k}$. An incremental displacement $\delta\Delta$ was generated and the incremental load δT and prying force δQ are calculated as shown below

$$\delta T = K_{ij,k}\delta\Delta \tag{38}$$

$$\delta Q = KQ_{ij,k}\delta\Delta \tag{39}$$

Considering force equilibrium of the system, the force in the bolts, B, after pretension has been overcome can be calculated as the sum of the applied load T and the prying force Q. Moment equilibrium of the system yield the following incremental values for each displacement increment

$$\delta B = \delta T + \delta Q \tag{40}$$

$$\delta M_{k-zone} = \delta Tm - \delta Qn \tag{41}$$

$$\delta M_B = \delta Qn \tag{42}$$

The initial incremental displacement was calculated as the minimum of

$$\delta\Delta_1 = \frac{\delta B}{K_{ij,k} + Q_{ij,k}} \tag{43}$$

$$\delta\Delta_2 = \frac{\delta M_{k-zone}}{K_{ij,k} m + Q_{ij,k} n} \tag{44}$$

$$\delta\Delta_3 = \frac{\delta M_B}{Q_{ij,k} n} \tag{45}$$

When the prying is negative, the possibility of the endplate separating completely from the column flange must also be checked and the respective deformation of the flange is calculated as follows

$$\delta\Delta = \frac{-Q}{Q_{ij,k}} \tag{46}$$

Once the incremental forces and moments were calculated, $M_{k\text{-}zone}$, M_B and B were updated, compared to their corresponding limits, the stiffness and prying gradient were updated according to the new endplate state. At the *lower bolts* level, where full separation occurs the total bolt tensile force is calculated as $T' = \gamma\xi B$, and added to the *upper bolts* force, T, at every incremental step. The moment limits are simply the plastic moment at the K-zone $M_{pK\text{-}zone}$ and the bolt line M_{pB}

$$M_{pK-zone} = \frac{F_y p t_p^2}{4} \tag{47}$$

$$M_{pB} = \left(1 - \frac{d_h}{p}\right)\frac{F_y p t_p^2}{4} \tag{48}$$

The incremental process is applied in an iterative process. Figs. 12(a)-(b) show a comparison of the proposed endplate stiffness model versus FE results for extended endplate connections having circular bolt configuration associated with W30×108 and W 24×76 beams (where t_p = 2.5 cm). The proposed stiffness model predicts with excellent agreement the initial stiffness, onset of yielding, strength and deformation when compared with the FE results.

10.2.2 Column flange with circular bolt configuration

A stiffness model was developed to predict the response of the column flange having circular bolt configuration. As discussed earlier, the bolts were divided into three *Sets* (see Fig. 1(c)). The proposed stiffness model, of each bolt strip, consists of two bolts characterized by a spring and a beam element for the column flange in the transversal direction as shown in Fig. 6(a). The total response of the column flange is obtained by assembling the contribution from each *Set* at common incremental loads. The force and displacement were calculated according to the iterative procedure discussed in the Section 10.2.1, where t_{cf} (cm) is equal to the column flange thickness (t_{cf} is considered instead of t_p), m (cm) the length the column flange measured from the inside edge

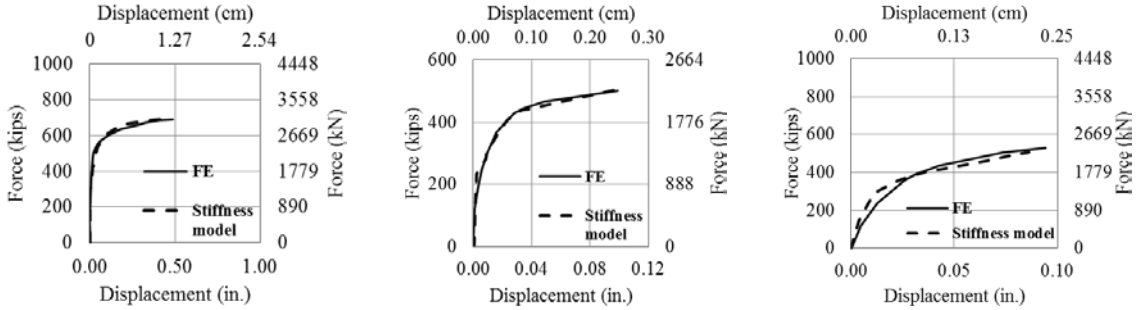

(a) Comparison of the FE results with the proposed extended endplate with circular bolt configuration stiffness model associated with W30x108 beam

(b) Comparison of the FE results with the proposed extended endplate with circular bolt configuration stiffness model associated with W24x76 beam

(c) Column flange stiffness model having circular bolt configuration associated with W30x108 beam connected to a W14x159 column (t_{cf} = 3.2 cm)

Fig. 12 Comparison of the FE results with the proposed extended endplate and column flange with circular bolt configuration stiffness model

of the bolt line to the location of the K-zone and *n* (cm), the length of the column flange measured from the inside edge of the bolt line to the point where contact occurs between the column flange and the endplate. The tributary width per bolt, *p*, was calculated as per Eq. (9). A linear interpolation is used to make sure that all the points from every *Set's* stiffness model are included in the total column flange force-deformation curve. A comparison of the force-deformation curve obtained from the proposed model and FE results for column flange having t_{cf} = 3.2 cm (1.25 in.) with circular bolt configuration is shown in Fig. 12(c). The proposed stiffness model predicts the force deformation response of the column flange with excellent agreement when compared with FE results.

10.3 Extended endplate/column system with rectangular bolt configuration

10.3.1 Extended endplate with rectangular bolt configuration

The extended endplate full response is modeled analytically on the basis of a beam representation for the endplate, a multi-linear spring for the bolts, accounting for the contact phenomenon (primary prying) that occurs between the endplate and the column flange assumed rigid and the beam web stiffening effect as shown in Fig. 6(b). The primary prying force at the tip of the plate was simulated using pin supports.

According to the detailed FE modeling performed as part of this study, at failure, plastification of the extended endplate occurred at the K-zone followed by interior bolt fracture at the level of the *upper bolts* (see Fig. 1(b)). Whereas, at the *lower bolts* level, the beam web stiffens the endplate which separates from the column flange (see Fig. 9). Hence the *lower bolts* are subject to pure tensile force. Fig. 11(b) shows the decision tree of the possible endplate limit states considered in this study. The system is loaded by applying a vertical force *T* at point A (K-zone) as shown in Fig. 6(b). The change of the reaction load at point C at every load increment is the prying gradient ΔQ, and the reaction load at failure of the bolts is the primary prying force *Q*. The ratio of the applied force, *T*, at point A (K-zone) to the displacement, Δ, of point A (K-zone) is the stiffness *K* of the endplate. The subscript used in the stiffness term reflects the plate limit state at the K-

zone and *upper bolts* line, and the limit state of the *upper bolts*.

For instance $K_{eee,kk}$ (see Fig. 11(b)), represents the stiffness of the endplate when it is in the elastic range, and the *upper bolts* are in their k^{th} stiffness range. Whereas the term $K_{pee,kk}$, represents the stiffness of the endplate when plastification occurred at the K-zone and the *upper bolts* are in their k^{th} stiffness step. The procedure was applied in an incremental computer automated iterative solution to simulate the mechanical response for mixed mode failure of the *upper bolts*. The change in the interior and the exterior *upper bolts* force ΔB_{int} *and* ΔB_{ext}, the change in the moment at the K-zone, $\Delta M_{K\text{-}zone}$ and the prying gradient, ΔQ, were generated within the software for different endplate limit states:

(1) Elastic limit state

$$\Delta Q = \frac{\Delta T}{\left(\frac{a^3\gamma_1}{6EI} - \frac{a\left(a+b+c\right)^2\gamma_1}{2EI} + \frac{\gamma_1\gamma_2 a^{\,2}c}{2EI\gamma_3} - \frac{f_s a\gamma_1}{GA} + \frac{\gamma_2}{\gamma_3} - 1 \right)} \tag{49}$$

$$\Delta B_{\text{int}} = \frac{\Delta Q\gamma_2}{\gamma_3} \tag{50}$$

$$\Delta B_{ext} = \left(\frac{\Delta Q a^3}{6EI} - \frac{\Delta Q a\left(a+b+c\right)^2}{2EI} + \frac{\Delta B_{int} ac^2}{2EI} - \frac{f_s \Delta Q a}{GA} \right)\gamma_1 \tag{51}$$

$$\Delta M_{K-zone} = \Delta T\left(b+c\right) - \Delta B_{int} b - \Delta Q a \tag{52}$$

$$K_{eee,kk} = \frac{1}{\gamma_7} \tag{53}$$

$$\gamma_1 = \frac{1}{\left(\frac{1}{K_{b1,k}} - \frac{a\left(b+c\right)^2}{2EI} \right)} \tag{54}$$

$$\begin{aligned} \gamma_2 = {} & \frac{\left(a+b\right)^3}{6EI} - \frac{a^3b^3\gamma_1}{36\left(EI\right)^2} + \frac{ab^3\left(a+b+c\right)^2\gamma_1}{12\left(EI\right)^2} + \frac{ab^3 f_s\gamma_1}{6EIGA} - \frac{\left(a+b\right)\left(a+b+c\right)^2}{2EI} \\ & + \frac{a^3\left(a+b\right)\left(b+c\right)^2\gamma_1}{12\left(EI\right)^2} - \frac{a\left(a+b\right)\left(b+c\right)^2\left(a+b+c\right)^2\gamma_1}{4\left(EI\right)^2} + \gamma_4 \end{aligned} \tag{55}$$

$$\gamma_3 = \left(\frac{1}{K_{b2,k}} + \frac{ab^3c^2\gamma_1}{12(EI)^2} - \frac{(a+b)c^2}{2EI} - \frac{ac^2(a+b)(b+c)^2\gamma_1}{4(EI)^2} - \frac{abc^2 f_s\gamma_1}{2GAEI} \right) \tag{56}$$

$$\gamma_4 = -\frac{a(a+b)(b+c)^2 f_s\gamma_1}{2GAEI} - \frac{(a+b)f_s}{GA} + \frac{a^3b_s\gamma f_1}{6EIGA} - \frac{a(a+b+c)^2 f_s\gamma_1}{2GAEI} - \left(\frac{f_s}{GA}\right)^2 ab\gamma_1 \tag{57}$$

$$\gamma_5 = \frac{a^3\gamma_1}{6EI} - \frac{a(a+b+c)^2\gamma_1}{2EI} + \frac{\gamma_1\gamma_2 a^2 c}{2EI\gamma_3} - \frac{f_s a\gamma_1}{GA} + \frac{\gamma_2}{\gamma_3} - 1 \tag{58}$$

$$\gamma_6 = \frac{a^3}{6EI\gamma_5} - \frac{a(a+b+c)^2}{2EI\gamma_5} + \frac{\gamma_2 ac^2}{2EI\gamma_3\gamma_5} - \frac{f_s a}{GA\gamma_5} \tag{59}$$

$$\gamma_7 = \left[\frac{(a+b+c)^3}{6\gamma_4} - \frac{\gamma_1\gamma_6(b+c)^3}{6} - \left(\frac{\gamma_2 c^3}{6\gamma_3\gamma_4}\right) + \gamma_8 \right]\left(\frac{1}{EI}\right) + \gamma_9 \tag{60}$$

$$\gamma_8 = \left(\frac{f_s}{GA}\right)\left(-\left(\frac{a+b+c}{\gamma_4}\right) + \gamma_1\gamma_6(b+c) + \left(\frac{\gamma_2 c}{\gamma_3\gamma_4}\right)\right) \tag{61}$$

$$\gamma_9 = \left(\left(\frac{-(a+b+c)^2}{2\gamma_4}\right) + \frac{\gamma_1\gamma_6(b+c)^2}{2} + \left(\frac{c^2\gamma_2}{2\gamma_3\gamma_4}\right)\right)(a+b+c) \tag{62}$$

(2) Plastic hinge formation at K-zone of plate limit state

$$\Delta Q = \Delta T\left(1 - \frac{b+c}{bK_{b2,k}\gamma_{10}} - \frac{b+c}{b}\right)\left(\frac{1}{\gamma_{11}}\right) \tag{63}$$

$$\Delta B_{int} = \frac{\Delta T(b+c)}{b} - \frac{\Delta Q a}{b} \tag{64}$$

$$\Delta B_{ext} = \left(\frac{\Delta B_{int}}{K_{b2,k}} - \frac{\Delta Q(a+b)^3}{6EI} - \frac{\Delta Q f_s(a+b)}{GA} + \frac{\Delta Q a^2(a+b)}{6EI} + \frac{\Delta Q f_s(a+b)}{GA}\right)\left(\frac{1}{\gamma_{10}}\right) \tag{65}$$

$$K_{pee,kk} = \frac{1}{\gamma_{14}} \tag{66}$$

$$\gamma_{10} = \left(\frac{a+b}{aK_{b1,k}} - \frac{b^3}{6EI} + \frac{f_s b}{GA} \right) \tag{67}$$

$$\gamma_{11} = \left(\frac{-a}{bK_{b2,k}\gamma_{10}} - \frac{(a+b)^3}{6EI\gamma_{10}} + \frac{a^2(a+b)}{6EI\gamma_{10}} - 2 \right) \tag{68}$$

$$\gamma_{12} = \left(1 - \frac{b+c}{bK_{b,2k}\gamma_{10}} - \frac{b+c}{b} \right)\left(\frac{1}{\gamma_{11}} \right) \tag{69}$$

$$\gamma_{13} = \frac{\frac{b+c-a\gamma_{12}}{b}}{K_{b,2k}} - \frac{(a+b)^3\gamma_{12}}{6EI} - \frac{f_s(a+b)\gamma_{12}}{GA} + \frac{a^2(a+b)\gamma_{12}}{6EI} + \frac{f_s(a+b)\gamma_{12}}{GA} \tag{70}$$

$$\gamma_{14} = \frac{(a+b+c)^3\gamma_{12}}{6EI} - \frac{(b+c)^3\gamma_{13}}{6EI\gamma_{10}} - \left(\frac{c^3}{6EI} \right)\left(\frac{b+c-a\gamma_{12}}{b} \right) + \gamma_{15} + \gamma_{16} \tag{71}$$

$$\gamma_{15} = \left(\frac{f_s}{GA} \right)\left((a+b+c)\gamma_{12} + (b+c)\left(\frac{\gamma_{13}}{\gamma_{10}} \right) + \left(\frac{b+c-a\gamma_{12}}{b} \right)c \right) \tag{72}$$

$$\gamma_{16} = \left(\left(\frac{1}{K_{b1,k}a} \right)\left(\frac{\gamma_{13}}{\gamma_{10}} \right) - \frac{a^2\gamma_{12}}{6EI} + \frac{f_s\gamma_{12}}{GA} \right)(a+b+c) \tag{73}$$

Where ΔT (kN) is the change in the applied load, a (cm) is the length of the plate measured from the inside edge of the interior bolt to the location of occurrence of the plastic hinge at the K-zone of the column flange, b (cm) is the gage distance between the tension bolts, c (cm) is the length of the plate measured from the inside edge of the exterior bolt line to the outside edge of the extended endplate, γ_1, γ_2, γ_3, γ_4, γ_5, γ_6, γ_7, γ_8, γ_9, γ_{10}, γ_{11}, γ_{12}, γ_{13}, γ_{14}, γ_{15} and γ_{16} are constants used in the calculation of the endplate stiffness, A (cm^2) is the cross sectional area, f_s is the shape factor used in computing the shear deformations, $K_{b1,k}$ (kN/cm) represents the stiffness of the interior bolt in the k^{th} step, and $K_{b2,k}$ (kN/cm) represents the stiffness of the exterior bolt in the k^{th} step.

The stiffness terms were derived to be applied in an incremental computer automated iterative solution. At the beginning the elastic stiffness of the flange $K_{eee,11}$ is calculated from structural analysis methods. Next, several checks need to be made to determine which limit state will be

reached first. The possible limit states are: (1) full plastification of the K-zone; (2) yielding of the interior bolt. Then, the prying gradient, the moment at the K-zone and the forces in the interior and exterior bolts corresponding to the current load step are computed. Finally, incremental displacement corresponding to the current load step is calculated, and the new stiffness is determined and the process is repeated again until the interior bolt force reaches $B_{fracture}$. After obtaining the load response for mixed mode failure of the *upper bolts* strength model, the bolt tensile force *T'* exhibited at the *lower bolts* level, was added to the total load at every step. At every incremental deformation Δ (cm), the bolt force is calculated as $B = K_{b,k}(\Delta)$, where $K_{b,k}$ is the corresponding bolt stiffness and $T' = \gamma n_b \zeta B/8$.

Figs. 13(a)-(b) show a comparison of the proposed stiffness model versus the FE results for endplate connection associated with W30×108 and W24×76 beams. The proposed stiffness model predicts with excellent agreement the initial stiffness, onset of yielding, strength and deformation when compared with the FE results.

10.3.2 Column flange with rectangular bolt configuration stiffness model

From the FE results, full plastification occurs at the level of the column flange with rectangular

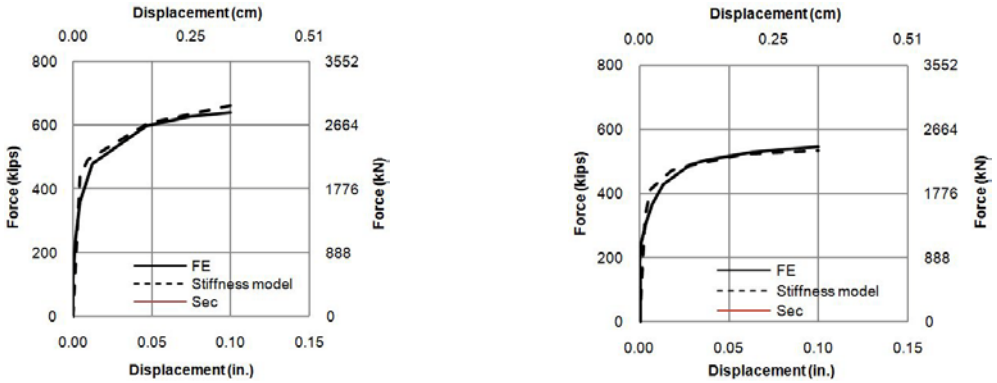

(a) Associated with W30×108 beam (b) Associated with W24×76 beam

Fig. 13 FE vs. proposed stiffness model extended endplate with rectangular bolt configuration

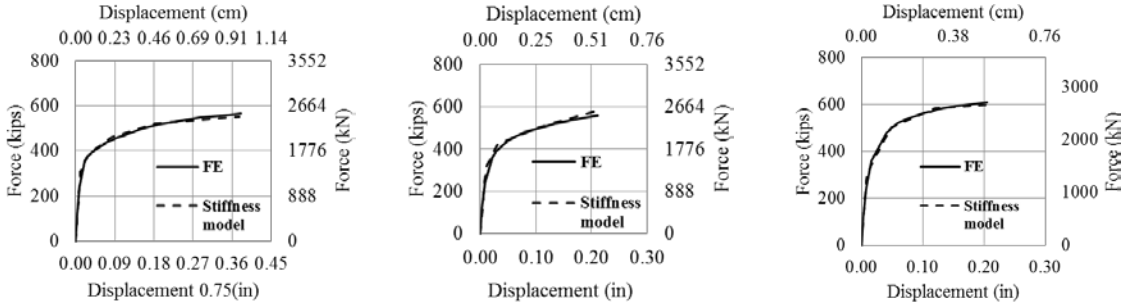

(a) t_{cf} = 1.9 cm (b) t_{cf} = 2.2 cm (c) t_{cf} = 2.5 cm

Fig. 14 FE vs. proposed stiffness model of column flange with rectangular bolt configuration associated with W30×108 beam

bolt configuration when t_{cf} varies between 1.9 cm (0.75 in.) and 3.2 cm (1.2 in.). The column flange was subdivided into strips consisting of two tension bolts modeled as shown in Fig. 6(a). Plastic hinge will develop at the k-zone followed by the plastification of the bolt lines. The same iterative process described in section 10.2.1 is applied to get the total response of the column flange, where $T' = T$.

Figs. 14(a)-(c) show a comparison of the proposed column flange stiffness model versus the FE results for endplate/column system associated with W30×108 girders having a column flange thickness t_{cf} equal to 1.9, 2.2, and 2.5 cm, respectively. The proposed stiffness model predicts with excellent agreement the initial stiffness, onset of yielding, strength and deformation when compared with the FE results.

11. Total assembly

After each of the different deformation mechanisms for the extended endplate and the column flange has been computed, the total force force-deformation curve of the connection is obtained by assembling the contribution from individual components at common incremental loads. Linear interpolation is used to make sure that all the load points from all the component stiffness models are included in the total force-deformation curve. Fig. 15 shows a comparison of the total force-deformation curve obtained from the stiffness model and FE results for (a) extended endplate connection with circular bolt configuration associated to W24×76 beam connected to a W14×159 column; and (b) extended endplate connection with rectangular bolt configuration associated to W30×108 beam connected to a W14×82. The proposed stiffness model predicts the force-deformation response of the extended endplate/column flange system with excellent agreement when compared to the FE results.

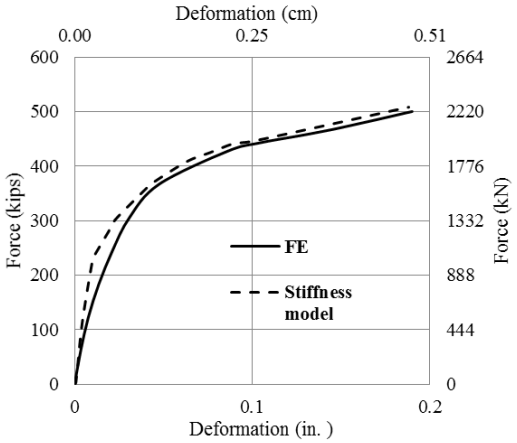

(a) Force-deformation of endplate connection with circular bolt configuration associated with W24×76 beam including column flange deformation: FE vs. Stiffness model

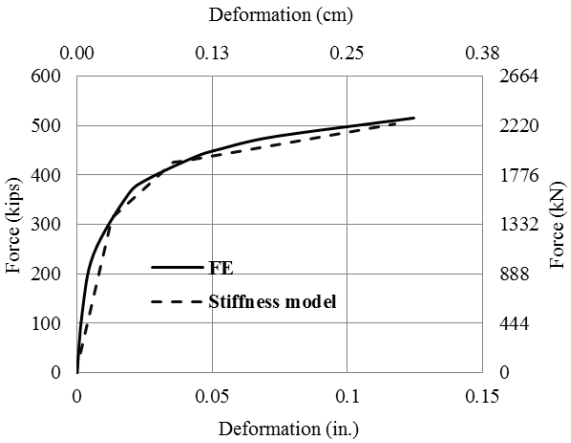

(b) Force-deformation of endplate connection with rectangular bolt configuration associated with W30×108 beam including column flange deformation: FE vs. Stiffness model

Fig. 15 FE vs. proposed stiffness model for endplate connection/column flange with circular and rectangular bolt configurations

12. Conclusions

When designing extended endplate connections associated with deep girders, it is necessary to identify and analyze all the yielding mechanisms and failure modes. In this research, a detailed design procedure is proposed for extended endplate with circular bolt configuration associated with deep girders. 3D nonlinear FE models were developed. A parametric study was conducted on 32 connections to investigate the effect of the circular bolt configuration on the prying phenomenon and bolt-force distribution. The prying force was quantified and analyzed based on FE results, validated with experimental results available in the literature. Extended endplate with circular bolt configuration exhibited larger prying forces when compared to its rectangular counterpart. Adopting a circular bolt configuration provides more overall ductile behavior. Strength and stiffness models that predict the deformation and capacity of the extended endplate/column flange system with circular and rectangular bolt configurations were developed. The proposed models show excellent agreement when comparing with FE and experimental results. Yield line theory was used to quantify the minimum column flange thickness requirement for the column with circular bolts pattern. One of the main advantages of the proposed models is that, in addition to its accuracy, it requires much less computational effort than that required using FE analysis, and can be used as well in more advanced modeling applications for seismic analysis and design. This study provides engineers guidelines to design extended endplate connections with circular bolt configuration.

Acknowledgments

The authors gratefully acknowledge the financial support provided by the American University of Beirut Research Board under grant No.103187-23310, and by the Lebanese National Council for Scientific Research (LNCSR) under grant No. 103091-22968.

References

Akgőnen, A.İ., Yorgun, C. and Vatansever, C. (2015), "Cyclic behavior of extended end-plate connections with European steel shapes", *Steel Compos. Struct., Int. J.*, **19**(5), 1185-1201.

ANSI/AISC Committee 358 (2010), Prequalified Connections for Special and Intermediate Steel Moment Frames for Seismic Applications; American Institute of Steel Construction 358-10, Chicago, IL, USA.

ANSI/AISC 360 (2010), Specification for Structural Steel Buildings; American Institute of Steel Construction 360-10, Chicago, IL, USA.

Bai, R., Chan, S.L. and Hao, J.P. (2015), "Improved design of extended end-plate connection allowing for prying effects", *J. Construct. Steel Res.*, **113**, 13-27.

Coelho, A.M.G., Bijlaard, F.S. and da Silva, L.S. (2004), "Experimental assessment of the ductility of extended end plate connections", *Eng. Struct.*, **26(**9), 1185-1206.

Comité Europènne de Normalisation CEN, (Ed.) (2005), EN 1993-1-1: Eurocode 3: Design of Steel Structures. Part 1-1: General Rules and Rules for Buildings; Eurocode 3, Brussels, Belgium.

Douty, R.T. and McGuire, W. (1965), "High strength bolted moment connections", *J. Struct. 725 Div.*, **91**(2), 101-128.

Faella, C., Piluso, V. and Rizzano, G. (1997), "A new method to design extended end plate connections and semirigid braced frames", *J. Construct. Steel Res.*, **41**(1), 61-91.

Ghassemieh, M., Baei, M., Kari, A., Goudarzi, A. and Laefer, D.F. (2015), "Adopting flexibility of the end-plate connections in steel moment frames", *Steel Compos. Struct., Int. J.*, **18**(5), 1215-1237.

Hantouche, E.G., Kukreti, A.R. and Rassati, G.A. (2012), "Investigation of secondary prying in thick built-up T-stub connections using nonlinear finite element modeling", *Eng. Struct.*, **36**, 113-122.
Hantouche, E.G., Kukreti, A.R., Rassati, G.A. and Swanson, J.A. (2013), "Modified stiffness model for thick flange in built-up T-stub connections", *J. Construct. Steel Res.*, **81**, 76-85.
Hantouche, E.G., Kukreti, A.R., Rassati, G.A. and Swanson, J.A. (2015), "Prying models for strength in thick-flange built-up t-stubs with complete joint penetration and fillet welds", *J. Struct. Eng.*, **141**(2), 04014102.
Hu, J.W., Leon, R.T. and Park, T. (2012), "Mechanical models for the analysis of bolted T-stub connections under cyclic loads", *J. Construct. Steel Res.*, **78**, 45-57.
Katula, L. and Dunai, L. (2015), "Experimental study on standard and innovative bolted end-plate beam-to-beam joints under bending", *Steel Compos. Struct., Int. J.*, **18**(6), 1423-1450.
Kiamanesh, R., Abolmaali, A. and Razavi, M. (2013), "Effect of circular bolt pattern on behavior of extended end-plate connection", *J. Struct. Eng.*, **139**(11), 1833-1841.
Kukreti, A.R., Murray, T.M. and Abolmaali, A. (1987), "End-plate connection moment-rotation relationship", *J. Construct. Steel Res.*, **8**, 137-157.
Lemonis, M.E. and Gantes, C.J. (2009), "Mechanical modeling of the nonlinear response of beam-to-column joints", *J. Construct. Steel Res.*, **65**(4), 879-890.
Liu, X. and Wang, Y. (2015), "Influence of extended end-plate connection construction parameters change on prying force in extended end plate", *World Inform. Earthq. Eng.*, **33**(3), 148-155.
Morrison, M., Schweizer, D. and Hassan, T. (2015), "An innovative seismic performance enhancement technique for steel building moment resisting connections", *J. Construct. Steel Res.*, **109**, 34-46.
Piluso, V. and Rizzano, G. (2008), "Experimental analysis and modelling of bolted T-stubs under cyclic loads", *J. Construct. Steel Res.*, **64**(6), 655-669.
Piluso, V., Faella, C. and Rizzano, G. (2001), "Ultimate behavior of bolted T-stubs. II: Model validation", *J. Struct. Eng.*, **127**(6), 694-704.
Pucinotti, R. (2001), "Top-and-seat and web angle connections: prediction via mechanical model", *J. Construct. Steel Res.*, **57**(6), 663-696.
Rassati, G.A., Leon, R.T. and Noe, S. (2004), "Component modeling of partially restrained composite joints]under cyclic and dynamic loading", *J. Struct. Eng.*, **130**(2), 343-351.
Schweizer, D.Q. (2013), "Experimental investigation of innovative seismic performance enhancement techniques for steel building beam to column moment connections", Ph.D. Dissertation; North Carolina State University, Raleigh, NC, USA.
Sumner, E.A. and Murray, T.M. (2002), "Behavior of extended end-plate moment connections subject to cyclic loading", *J. Struct. Eng.*, **128**(4), 501-508.
Swanson, J.A. (2002), "Ultimate strength prying models for bolted T-stub connections", *Eng. J.*, **39**(3), 136-147.

CC